The role of the copper oxidation state in the electrocatalytic reduction of CO_2 into valuable hydrocarbons

Juan-Jesús Velasco-Vélez[1,2]*, Travis Jones[2], Dunfeng Gao[3,4], Emilia Carbonio[2], Rosa Arrigo[5,6], Cheng-Jhih Hsu[7], Yu-Cheng Huang[7,8], Chung-Li Dong[7], Jin-Ming Chen[8], Jyh-Fu Lee[8], Peter Strasser[9], Beatriz Roldan Cuenya[3,4], Robert Schlögl[1,2], Axel Knop-Gericke[1,2], Cheng-Hao Chuang[7]*

*Corresponding authors: velasco@fhi-berlin.mpg.de, chchuang@mail.tku.edu.tw

[1]Department of Heterogeneous Reactions, Max Planck Institute for Chemical Energy Conversion, Stiftstraße 34-36, Mülheim an der Ruhr 45470, Germany

[2]Department of Inorganic Chemistry, Fritz-Haber-Institut der Max-Planck-Gesellschaft, Faradayweg 4-6, Berlin 14195, Germany

[3] Department of Physics, Ruhr-University Bochum, Universitätstraße 150, 44780 Bochum, Germany

[4]Department of Interface Science, Fritz-Haber-Institute of the Max-Planck Society, Faradayweg 4-6, 14195 Berlin, Germany

[5]Diamond Light source Ltd., Harwell Science & Innovation Campus, Didcot, Oxfordshire OX 11 0DE, UK

[6]School of Environment and Life Sciencesm, University of Salford, Cockcroft building, M5 4WT, Manchester, UK

[7]Department of Physics, Tamkang University, No. 151 ,Yingzhuan Rd., Danshui Dist, New Taipei City 25137, Taiwan.

[8]National Synchrotron Radiation Research Center, No. 101, Hsin Ann Rr., East District., Hsinchu 30076, Taiwan

[9]Department of Chemistry, Chemical Engineering Division, Technical University Berlin, Straße des 17. Juni 124, 10623 Berlin, Germany

Abstract: Redox-active copper catalysts with accurately prepared oxidation states (Cu^0, Cu^+ and Cu^{2+}) and high selectivity to C_2 hydrocarbon formation, from electrocatalytic cathodic reduction of CO_2, were fabricated and characterized. The electrochemically prepared copper-redox electro-cathodes yield higher activity for the production of hydrocarbons at lower oxidation state. By combining advanced X-ray spectroscopy and *in situ* micro-reactors it was possible to unambiguously reveal the variation in the complex electronic structure that the catalysts undergo at different stages (i.e. during fabrication and electrocatalytic reactions). It was found that the surface, sub-surface and bulk properties of the electrochemically prepared catalysts are dominated by the formation of copper carbonates on the surface of cupric-like oxides, which prompts catalyst deactivation by restraining effective charge transport. Furthermore, the formation of reduced or partially-reduced copper catalysts yields the key dissociative proton-consuming reactive adsorption of CO_2 to produce CO; allowing the subsequent hydrogenation into C_2 and C_1 products by dimerization and protonation. These results yield valuable information on the variations in the electronic structure that redox-active copper catalysts undergo in the course of the electrochemical reaction, which, under extreme conditions are mediated by thermodynamics but, critically, kinetics dominate near the oxide/metal phase transitions.

Keywords: CO_2RR, electrodeposited prepared copper oxides, *in situ* X-ray spectroscopy, copper carbonate passivation layer, charge transport limitation, DFT calculations, electrocatalytic active reduced copper oxides.

Introduction

Many solutions have been proposed to minimize the impact of CO_2 emissions, such as its sequestration or its chemical transformation into value added industrial products[1,2]. Among other technologies, the electrocatalytic route of energy conversion becomes of great importance because the electricity produced by renewable sources, like solar and wind, can be used to transform CO_2 into various chemical feedstocks[3,4]. In this direction, over the last decades different materials capable of electrochemically reducing CO_2 in aqueous solution to produce hydrocarbons have been identified[5]. Unfortunately, none of these materials are efficient and stable enough for practical use[6]. Copper is unique in its ability to electro-reduce CO_2 to hydrocarbons and alcohols in aqueous electrolytes, as was shown by Hori et al.[7,8]. However, the selective reduction of CO_2 into fuels is very challenging due to the multiple complex proton-coupled electron transfer steps that must occur[9]. This complex network makes the cathodic CO_2 reduction reaction (CO_2RR) suffer from relative low current density (CO_2RR competes with hydrogen evolution), high overpotential (cathodic and anodic)[10] and electrode deactivation/poisoning over time[11]. Hence, the CO_2RR has been investigated using a multitude of copper based electrodes fabricated in many different ways including single crystals[12], oxide-derived copper (OD-Cu)[13], nanowires[14],

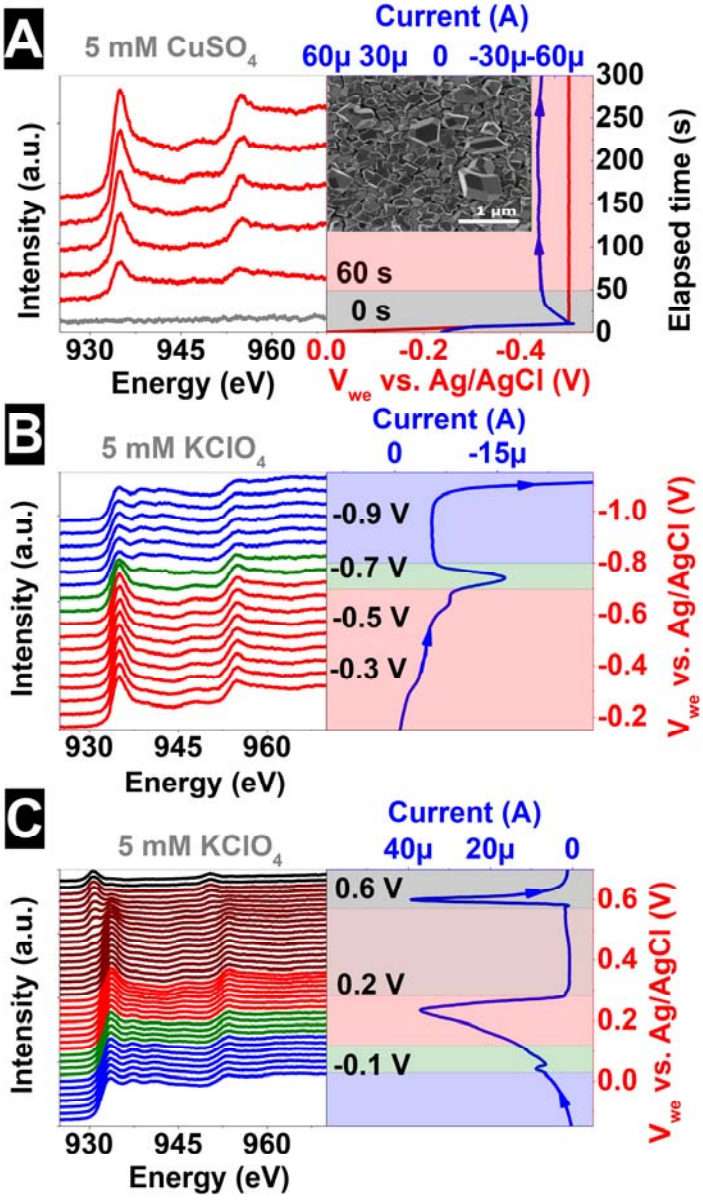

Figure 1: Cu $L_{2,3}$-edges XAS spectra and respective electrochemical current/voltage relations (bottom) during: **A** electrodeposition of Cu at -0.5 V vs. Ag/AgCl in 5 mM $CuSO_4$ in the time domain (inset SEM image of the electrodeposited copper electrode), **B** Electro-reduction of the electrodeposited Cu in 5 mM $KClO_4$. **C** Electrochemically controlled preparation of the electrodeposited Cu film in three different Cu oxidation states (Cu^0, Cu^+, Cu^{2+}).

electrodeposited[15], plasma treated foils[16], nanoparticles[17], porous hollow fibers[18], shaped particles[19-21], mesopores[22], and dendrites[23]. Nevertheless, the lack of detailed information on the electronic structure of these Cu surfaces during both the fabrication process and under the catalytic reaction makes it difficult to design more efficient and stable electrocatalysts[24]. Herein, we report on the preparation of catalysts highly selective to C2 hydrocarbon production and on the *in situ* monitoring of their electronic structure during preparation and electrocatalytic reaction. By tracking the electronic structure of the Cu catalysts, we were able to tune and precisely set the initial Cu redox state, such as Cu^0, Cu^+ and Cu^{2+}, by controlled applied potential protocols. Also, we traced the variations and modifications in the electronic structure (oxidation state) of the Cu catalysts during applied potential scans or steps and, in particular, under catalytic CO_2RR conditions. These experiments yielded unambiguous information of the catalyst redox processes governing the CO_2RR, as well as the nature of the active sites. In addition, the active/inactive and stable/unstable oxidation states depending on the applied potential and electrolyte were revealed.

Experimental section

Electrode preparation: The copper electrode was prepared by electrodeposition from 5 mM $CuSO_4$. The electrolyte was prepared by diluting 0.798 g of $CuSO_4$ (Sigma Aldrich, anhydrous powder, 99.99%) in 1 liter of Milli-Q water (18.2 MΩ) at room temperature (RT), 25°C. The electrolyte was continuously saturated with pure N_2 gas by bubbling it through the electrolyte containing the copper salts. Therefore, the electrode was deposited at -0.5 V vs. Ag/AgCl yielding an overpotential deposition of copper in the oxidation state Cu^+. After the electrodeposition the electrolyte was changed to 5 mM of $KClO_4$ in order to reduce the surface to Cu^0. The electrolyte was prepared by diluting 0.372 g $KClO_4$ (Sigma Aldrich, 99%) in 1 liter of Milli-Q water (18.2 MΩ) at room temperature (RT), 25°C. The electrolyte was continuously saturated with pure N_2 gas by bubbling. After that, the electrode was anodically polarized to produce Cu^0, Cu^+ or Cu^{2+}-like oxides that were used during the *in situ* CO_2RR characterization. The X-ray absorption spectra at the Cu $L_{2,3}$-edges collected as functions of the applied potential during linear sweep voltammetry (LSV) used a 0.833 mV/s scan rate yielding a potential resolution amounting to 0.05 V (the acquisition time was one minute for each spectrum in "fly mode"). The spectra shown in Figure 1C have a resolution of 0.02 V, which was collected at a higher voltage resolution to ensure accurate control of the oxidation state.

Calculation methods: DFT calculations were performed with the Quantum ESPRESSO[37] package using the Perdew, Burke, and Ernzerhof (PBE) exchange and correlation potential[38]. Projector Augmented-Wave sets were taken from the PSLibrary[39] using a planewave basis set with a kinetic energy cutoff of 30 Ry (300 Ry) for wavefunctions. We tested the role of dispersion corrections using the exchange-hole dipole moment model[40] (XDM) for both the clean Cu (111) and the Cu (111) with oxygen in the subsurface octahedral hole. On the clean surface the activation energy was 1.68 eV with and without dispersion corrections whereas with

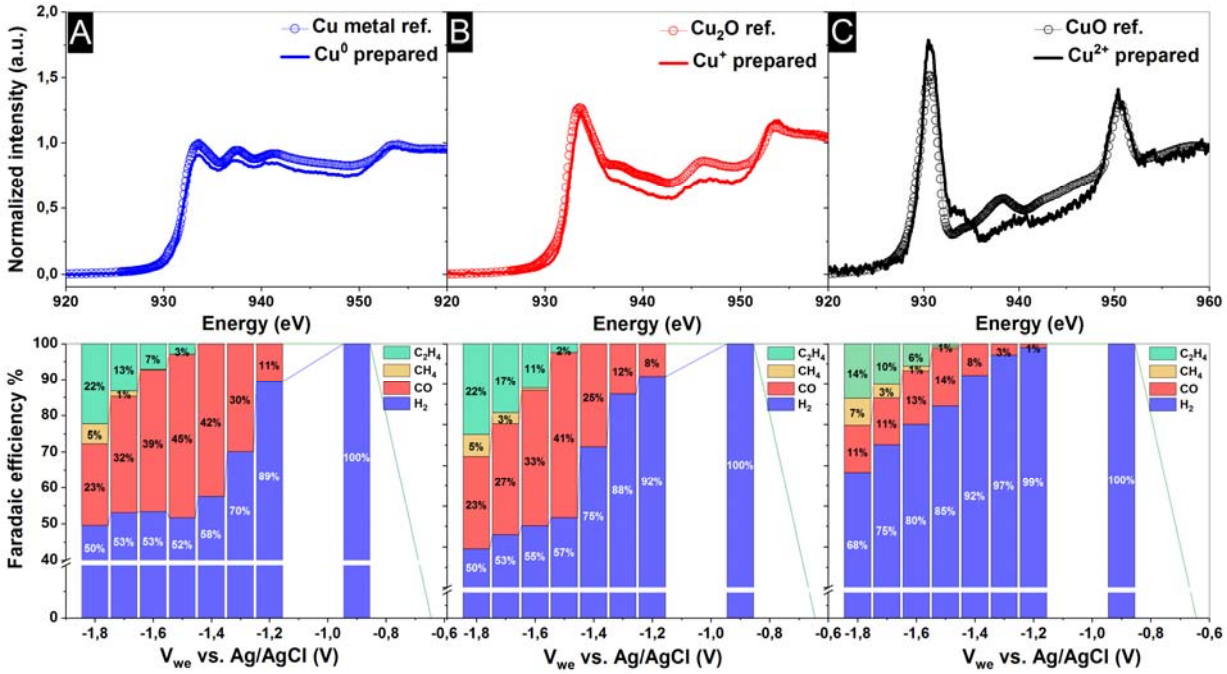

Figure 2: Cu $L_{2,3}$-edges spectra of electrochemically prepared Cu oxides (solid line) and their comparison with reference samples (circles) and potential-dependent Faradaic efficiency of the main products of the CO_2RR over *in situ* electrodeposited Cu films obtained on samples with the following starting chemical states: **A** Cu^0, **B** Cu^+ and **C** Cu^{2+}.

subsurface oxygen the activation energy was 1.54 eV with and 1.56 eV without dispersion corrections. Due to the small influence on barriers we chose to ignore dispersion corrections in the main text. Calculations on metallic copper employed a ***k***-point mesh equivalent to (12×12) for the (111) surface unit cell while those on Cu_2O employed a mesh equivalent to (2×4) for the (110) surface unit cell. In all cases Marzari-Vanderbilt[41] smearing was used with a smearing parameter of 0.02 Ry. For the Cu (111) surface we employed a 5 layer (2×2) surface unit cell slab with an in-plane lattice parameter of 5.15 Å. In the case of Cu_2O a four layer (2×2) slab was used with in-plane cell parameters of 12.02 and 8.50 Å. In all cases approximately 20 Å of vacuum was included to separate slabs from their periodic images and the bottom two layers were held fixed during ionic relaxation. MEPs were computed using the climbing image nudged elastic band method using 8 images for the metallic calculations and 16 images for those on Cu_2O. The transition states were converged when the force on the climbing image was less than 0.05 eV/Å and the energy change dropped below 10^{-3} eV.

CO_2 electroreduction measurements: CO_2 electroreduction measurements were carried out in a gas-tight H-cell separated by an anion exchange membrane (Selemion AMV, AGC Inc.). Both, the working electrode and counter electrode compartments were filled with 40 mL 0.1 M $KHCO_3$ (Honeywell Fluka, 99.7%) and purged continuously with CO_2 (99.995%, 20 mL min^{-1}). A $KHCO_3$ solution was prepared with ultrapure water and further pre-purified with Chelex 100 Resin (Bio-Rad, 100−200 mesh)[42]. Prior to the measurement, the electrolyte was bubbled with

CO_2 for 30 min to remove oxygen in the solution and saturate the solution. A platinum gauze (MaTecK, 3600 mesh cm^{-2}) was used as the counter electrode and a leak-free Ag/AgCl/3.4 M KCl electrode (Innovative Instruments, Inc.) was used for the reference electrode. The sample (Cu electrodeposited on Au mesh) was used as a working electrode and was contacted with a clamp wrapped by Kapton tape to avoid unwanted reactions. The sample was measured during CO_2RR at a constant potential for 1 h before changing to the next potential. The potentials were controlled with an Autolab potentiostat (PGSTAT 302N). The gas products were analyzed by online gas chromatography (GC, Agilent 7890A) every 17 min. CO, H_2, and hydrocarbons were separated by different columns (Molecular sieve 13X, HayeSep Q, and Carboxen-1010 PLOT) and quantified by a thermal conductivity detector (TCD) and flame ionization detector (FID). The reported Faradaic efficiency was calculated on the basis of the product distribution and current after 1 h of reaction at constant potential (see SI for calculations).

Results and Discussion

The electrocatalysts were prepared and characterized using X-ray absorption spectroscopy (XAS) measured in fluorescence yield (FY) mode in an *in situ* electrochemical cell; the setup described in the supported information (SI)[25]. While in general XAS-FY are not analogous to the X-ray absorption cross section at the $L_{2,3}$ edges due to their sensitivity to distinct FY decay channels, these differences are negligible for Cu in oxidation states below 3^+.[43] Thus, we will are free to compare XAS-FY to XAS and, as such, we will make no distinction between the two. The *in situ* XAS technique ensures an accurate direct correlation of the Cu redox state as a function of the applied potential, elapsed time and electrolyte. Copper electrodes were electrochemically deposited from 5 mM of $CuSO_4$ (4.8 pH) at -0.5 V vs. Ag/AgCl[26]. The voltammetric profile of the electrodeposition of Cu is shown in Figure 1A as function of the elapsed time. This process yields the electrodeposition of a stable oxy-hydroxide copper electrode (Cu^+), as the intense peak at 930.6 eV[27,28] in the XA spectrum indicates (highlighted in red). In order to minimize the impact of hydroxyl species on the electrodeposited copper electrode and to prepare a reproducible redox state, the deposited Cu electrode film was polarized cathodically in 5 mM $KClO_4$ (7 pH) to reduce Cu^+ to Cu^0, as shown in Figure 1B. The spectra collected as a function of applied potential confirm that the electrode reduces from Cu^+ (highlighted in red) to Cu^0 (highlighted in blue). This process is driven by the coupled ionic transport in solids in the presence of an applied electric field where the material acts as a solid-state electrolyte as well as a nonstoichiometric compound with mobile defects, like oxygen vacancies[29]. Diffusion is a slow process in solids, however the existence grain domains in our electrode facilitates diffusion due to the small grain size. Finally, after the electrochemical reduction of the deposited Cu film electrodes, the Cu oxidation state was deliberately controlled by linear sweep voltammetry (LSV) and concomitant recording of the electronic structure via *in situ* XAS at the Cu $L_{2,3}$-edges (Figure 1C). Stable Cu^{2+} species were produced under anodic polarization where a significant amount of Cu^{2+} dissolves due to a local reduction of the pH[27]. This dissolution diminished the thickness of the electrodeposited material somewhat. Using the

deposition and voltammetric post-treatment protocol above described, Cu electrodes in controlled distinct redox states, such as metallic copper (Cu^0, highlighted in blue), cuprous (Cu^+, highlighted in red) or cupric (Cu^{2+}, highlighted in dark) were reproducibly/accurately prepared. The electrosynthesis also resulted in the formation of a continuous electrode film composed of polyhedric particles with well-defined facets, as shown in the SEM image in the inset of Figure 1A. The accuracy of the oxidation state of the electrochemically prepared Cu electrode was verified by comparison with reference samples, Cu single crystal (Cu^0), cuprous oxide (Cu^+) and cupric oxide (Cu^{2+}), as shown in Figure 2.

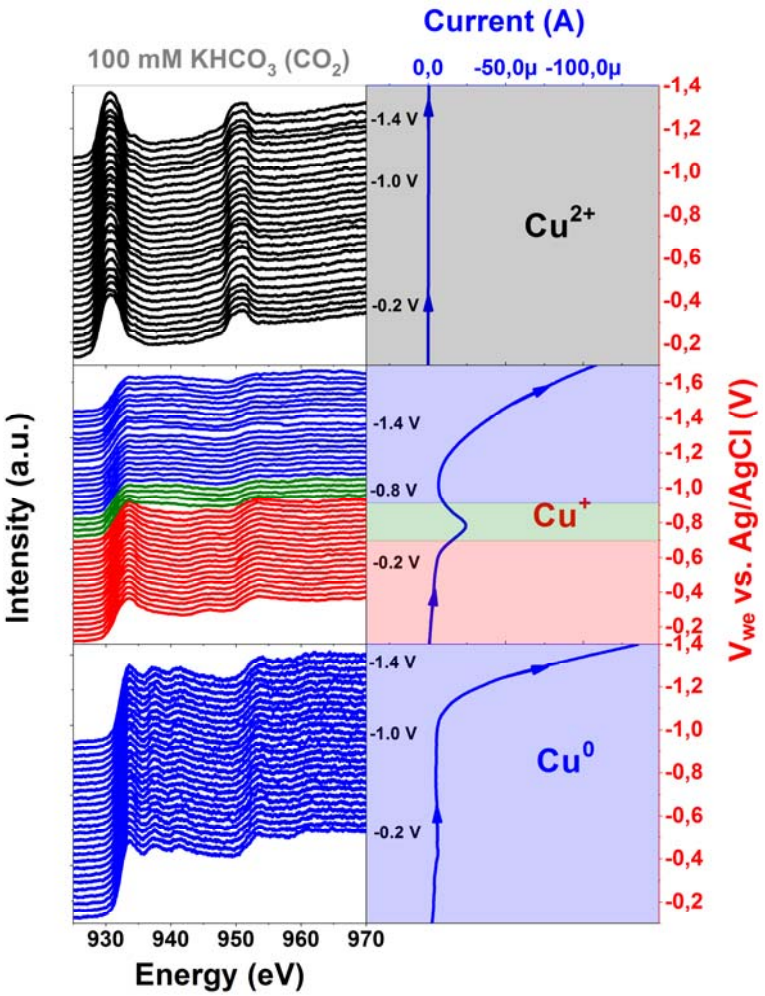

Figure 3: Cu $L_{2,3}$-edges spectra depending on the cathodic polarization in a 100 mM $KHCO_3$ solution saturated with CO_2(gas) and different initial oxidation state: Cu^0, Cu^+ and Cu^{2+} catalysts.

Next, the electrocatalytic CO_2 reduction activity of the Cu^{2+}, Cu^+ and Cu^0 film electrodes was investigated using online gas chromatography. The catalytic product distributions as function of applied electrode potentials for copper metal (Cu^0), cuprous like oxide (Cu^+) and cupric like oxide (Cu^{2+}) catalysts are shown in Figure 2A, 2B and 2C, respectively. The metallic Cu-like surface evolved hydrogen starting at -0.9 V vs. Ag/AgCl, followed by CO at -1.2 V vs. Ag/AgCl, which then forms CH_4, C_2H_4 at more cathodic potentials and small amounts of C_2H_6 (not shown), prompting a decline in the Faradaic efficiency of H_2 and CO. The Cu^+-like oxide behaves similar to the Cu^0 electrodes (Figure 2B), while the distribution of carbonaceous products for Cu^{2+} is lower, as shown in Figure 2C. Therefore, the electrodeposited catalysts show higher Faradaic efficiency to the formation of C_2 hydrocarbons where the Cu^0- and Cu^+-like catalysts are more active than the Cu^{2+}-like catalyst. To follow the time evolution of the redox state of the copper metal (Cu^0), cuprous oxide (Cu^+) and cupric oxide (Cu^{2+}) film catalysts under reaction conditions, we tracked the variations in electronic structure (in the Cu $L_{2,3}$-edges) under cathodic

potentials[30], both in CO_2-free (5 mM $KClO_4$, 7 pH) and different CO_2-saturated electrolytes (100 mM $KHCO_3$ pH 6.8, and 5 mM $KHCO_3$ 6 pH) :

i) Firstly, the performance of the electrochemically prepared metallic copper electrode was investigated in the presence of the three electrolytes: 5 mM $KClO_4$ saturated with N_2 gas (Figure S1A1), 5 mM $KHCO_3$ saturated with CO_2 gas (Figure S1A2), and 100 mM $KHCO_3$ saturated with CO_2 gas (Figure 3, bottom). From Figure 3 it is obvious that in the presence of N_2 (in 5 mM $KClO_4$ electrolyte) the electronic structure of the Cu^0 electrode remains unaltered over the entire potential range, as shown in Figure S1A1. When the applied potential reaches -1.1 V vs. Ag/AgCl the LSV shows an increase in the cathodic current ascribed to the Faradaic process with no evidence for the existence of copper oxide (within the FY photodetector limit). On the other hand, when the Cu^0 electrode is in the presence of CO_2 in 5 mM $KHCO_3$ electrolyte, the data show evidence for the formation of Cu^+ species that could be associated with the dissociative proton-consuming reactive adsorption of CO_2 on copper yielding chemisorbed CO (see Figure S1A2). Furthermore, this behavior is confirmed in Figure S2, where the increase in the main peak at 930.6 eV is induced by the presence of CO_2, which, from the Cu Pourbaix diagram, is ascribed to a $Cu+H_2O \rightarrow Cu_2O+2e^-+2H^+$ process. The same trends are observed at 100 mM $KHCO_3$, where the potential range was also extended to higher cathodic polarization (see Figure 3 bottom). The adsorption of CO on the copper surface is also corroborated by the cathodic peak in the LSV at around -0.4 V vs. Ag/AgCl. Furthermore, at higher potential, the CO is subsequently reactively desorbed from the surface, around -0.8 vs. Ag/AgCl, due to the competitive discharge of H^+ and the associated evolution of molecular H_2.

ii) As a second case, the behavior of the cuprous oxide-like electrode (Cu^+) was monitored during the identical cathodic voltammetric scan as the metallic electrode described previously. In the presence of N_2 (in 5 mM $KClO_4$ electrolyte) the cuprous-like oxide underwent a chemical reduction from Cu^+ to Cu^0 at -0.8 V vs. Ag/AgCl, as shown in Figure S1B1 where the reduction from Cu^+ to Cu^0 at a pH of 7 is expected to happen at -0.6 V vs. Ag/AgCl according to the Pourbaix diagram. However, in the presence of $KHCO_3$ electrolyte saturated in CO_2 the electrode behaves similar to the CO_2 free electrolyte, as proved in Figure S1B2 (5 mM $KHCO_3$) and Figure 3 (middle) (100 mM $KHCO_3$). Nevertheless, there was a slight decrease in the reduction potential peak position (in the LSV) ascribed to the transition from Cu^+ to Cu^0 at around -0.75 V vs. Ag/AgCl (highlighted in green). It is related to a noticeable increase in the redox current yielding a reduction wave in the LSV at -0.75 V vs. Ag/AgCl.

iii) Finally, the behavior of cupric-like oxide (Cu^{2+}) was elucidated during negative potential scans. In the presence of a CO_2 free electrolyte (5 mM $KClO_4$ saturated with N_2 gas) there were two reduction peaks at -0.2 V and -0.9 V vs. Ag/AgCl related to the reduction of Cu^{2+} to Cu^+ and of Cu^+ to Cu^0 respectively, as proved by the *in situ* XAS color maps in Figure S1C1. On the other hand, when cupric oxide was exposed to 5mM $KHCO_3$ saturated in CO_2 the less cathodic reduction wave (at -0.2 V vs. Ag/AgCl) in the LSV was suppressed (see Figure S1C2) due to the formation of highly stable/inert passivating copper carbonates[31]. As a result of this

passivation, copper remained in its Cu^{2+} oxidation state until it was reduced directly to Cu^0 at around -0.7 V vs. Ag/AgCl, showing the coexistence of Cu^{2+} and Cu^0 species during the reduction process, which is expected under high cathodic polarizations in a basic medium according to the Pourbaix diagram. Furthermore, when the electrolyte is changed to higher potassium carbonate concentration, i.e. 100 mM $KHCO_3$, a more stable copper carbonate layer is formed on the surface and cathodic reduction is suppressed, hindering charge transport, as shown in the upper panel of Figure 3. Note that the contact area of the working electrode is small in the *in situ* XAS electrochemical cell yielding high electrode contact resistance. This resistance can be lowered by increasing the working electrode area, which is planned for future electrochemical cell designs. Meanwhile, it is not a problem for the employed cell to detect the reaction products during online GC or for the *in situ* EXAFS electrochemical cell, which uses a larger SiN_x window area as indicated in the SI. For completeness, the stability of the formed copper carbonate layer was investigated in an acidic environment (100 mM $HClO_4$, 1 pH) as a function of time at open circuit voltage (OCV), as shown in Figure S3. These results indicate that the carbonate layer (probably azurite/malachite like, $Cu_3(CO_3)_2(OH)_2$/ $Cu_2CO_3(OH)_2$) remains stable for a long time even under harsh acidic conditions, which effectively hinders the charge transport between counter and working electrodes. Comparing the LSVs for the different Cu oxides, it is obvious that the lowest over-potentials and highest currents are achieved with the metal-like electrodes, Cu^0. On the other hand, Cu^{2+}-like oxides show low currents compatible with severe charge-transport limitation effects.

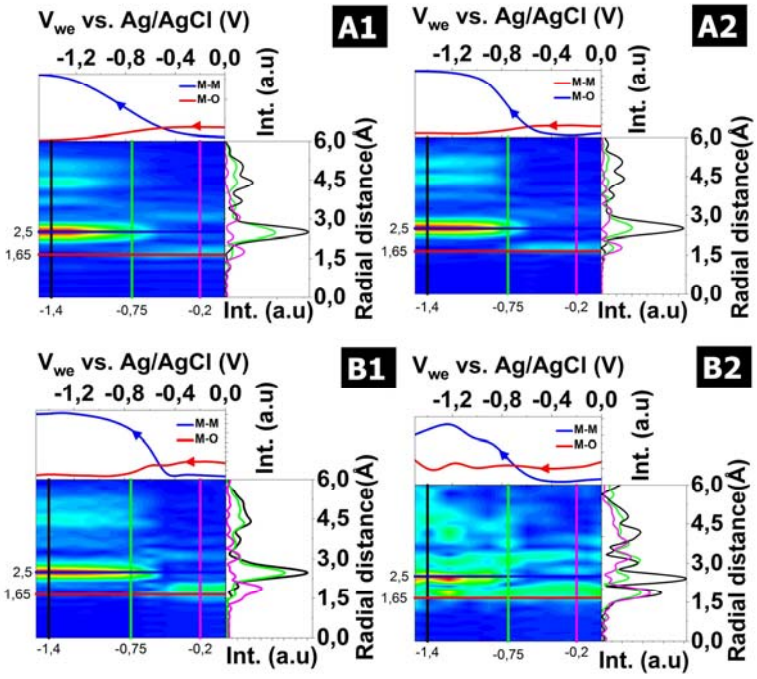

Figure 4: Fourier transformation analysis of EXAFS data: **A1** Cu^+ in the presence of 5 mM $KClO_4$ (N2) and **A2** Cu^+ in the presence of 100 mM $KHCO_3$ saturated with CO_2(gas). **B1** Cu^{2+} in the presence of 5 mM $KClO_4$ (N2) and **B2** Cu^{2+} in presence of 100 mM $KHCO_3$ saturated with CO_2(gas).

In order to verify the formation of passivating copper carbonates, *in situ* EXAFS measurements at the Cu K-edge were performed under reaction conditions for the Cu^+ and Cu^{2+}-like catalysts to obtain information about the metal-oxide (M-O) and metal-metal (M-M) bond distances. For the Cu K-edge measurements, each spectrum was collected at a fixed potential with an acquisition time of 1 hour, comparable to the GC product analysis acquisition times.

Figure 4A1 shows the EXAFS analysis of the Cu^{+}-like oxide as a function of applied potential in 5 mM $KClO_4$ saturated in N_2. It is obvious that initially the dominant species is a Cu^{+} oxide with a M-O distance dominant of around 1.65 Å. At increasing cathodic polarization, cuprous oxide underwent a reduction and the EXAFS spectra only show M-M distances (at around 2.5 Å), indicating the absence of any dominant oxide character at high cathodic polarization, in agreement with the Cu $L_{2,3}$-edges. When the electrolyte is changed to 100 mM $KHCO_3$ the behavior is similar; there is a dominant M-M distance at high cathodic polarization. However, a slight amount of oxygen remains with the characteristic M-O distance seen in Figure 4A2, which is ascribed to oxygen dissolved in the bulk and/or in subsurface of the material.

The cupric-like (Cu^{2+}) oxide was investigated under the same conditions as the cuprous-like oxide, and in the presence of the CO_2 free electrolyte the same trends as those seen for Cu^{+} are observed. A prominent peak at 2.5 Å is ascribed to the M-M distance, as shown in Figure 4B1, as the catalyst is reduced to metal at high cathodic polarization. Exposing the Cu^{2+}-like oxide electrode to a 100 mM $HKCO_3$ electrolyte saturated with CO_2, however, yields completely different behavior compare to the case of CO_2 free electrolyte. When the electrolyte is saturated with CO_2 there are two peaks under high cathodic polarization, see Figure 4B2. The M-M distance that evolves upon the electrode is reduced, and an M-O distance remains over the entire potential range. This lattice distance is ascribed to the copper carbonate species that hinder charge transport and dissociation of CO_2 into CO, thereby preventing hydrogenenation processes, in agreement with the Cu $L_{2,3}$-edges measurements. Note that the structural changes observed in the EXAFS measurements are not observed in the XA spectra at high cathodic potentials (Figure 3), as we discussed previously. It is due to the fact that the working electrode area is smaller in the XAS cell than in the EXAFS cell yielding a higher contact resistance, which hinders effective charge transport and saturates the potentiostat for the XAS cell.

Taking into account the discussed experiments, it is clear that the hydrogenation of carbon takes places when copper is mostly reduced whereas the cupric-like oxide is most likely inactive. *In situ* X-ray spectroscopies, both XAS and EXAFS, indicate that surface copper carbonates generated on cupric-like oxide form a passivation layer that hinders charge transport, thereby making Cu^{2+} inactive in the cathodic reduction of CO_2 into valuable hydrocarbons. As a result, Cu^{+} and Cu^{0} formation are required for activation. If the electrode is in the copper metal or cuprous oxide redox state, however, carbonate formation does not take place and the CO_2 can be reduced allowing its subsequent hydrogenation at higher cathodic potentials. While the nature of the hydrogenation products depends on the coverage of adsorbed intermediates—the first product evolved is C_2H_4 due to a dimerization process and finally CH_4 evolves due to protonation effects on a proton rich surface—it is expected that a key reaction step in the CO_2RR is the dissociation of CO_2 into CO. The magnitude of this dissociation barrier will likely depend on the degree of surface oxidation and nature of surface defects. Therefore, we calculated the barrier associated with dissociative CO_2 adsorption ($CO_{2,ads} \rightarrow CO_{ads} + O_{ads}$) on several copper catalysts, as shown in Figure 5, to test how the degree of surface reduction affects dissociative

CO_2 adsorption. As may be expected based on metallic surfaces[32], we found the activation energy for adsorption follows a Brønsted–Evans–Polanyi relation, that is, the CO dissociation barrier is linearly correlated with the heat of reaction ($E_{product}$-$E_{reactant}$) on different copper surfaces (Note that, for simplicity, the dissociation barrier was calculated without a specific assumption about the hydroxylation degree of the electrode and in the absence of electrolyte). At 1.68 eV, the metallic surface had one of the highest barriers for CO_2 decomposition with an associated heat of reaction (H_{rxn}) of 0.93 eV, where the positive sign indicates the reaction is endothermic. The presence of subsurface oxygen generally lowers this barrier by decreasing the endothermicity of H_{rxn}. In particular, when oxygen is present in the subsurface tetrahedral holes, shown in Figure 5, Cu(111)/O_{tet}, H_{rxn} drops to 0.77 eV with a concomitant drop in E_a to 1.55 eV. This change can be ascribed to the stability of the linear Cu-O-Cu bond in the product state[33], see Figure 5. Similarly, when oxygen is present in the subsurface octahedral hole, Cu(111)/$O_{oct(I)}$, E_a is 1.56 eV and H_{rxn} is 0.83 eV. In this case the decrease in H_{rxn} relative to the clean surface is not due to linear Cu-O-Cu bonding in the final state but to the binding of CO to the Cu^+ formed by the subsurface oxygen, see Figure 5. This can easily be verified by considering an alternative reaction path, Cu(111)/$O_{oct(II)}$, where the final state contains neither linear Cu-O-Cu bonding nor CO adsorption on Cu^+. In this case, at 2.2 eV, E_a is higher than on the clean surface due to more endothermic nature of the reaction (H_{rxn}=0.83 eV). Thus, an accumulation of subsurface oxygen is predicted to enhance CO_2 decomposition[34,35].

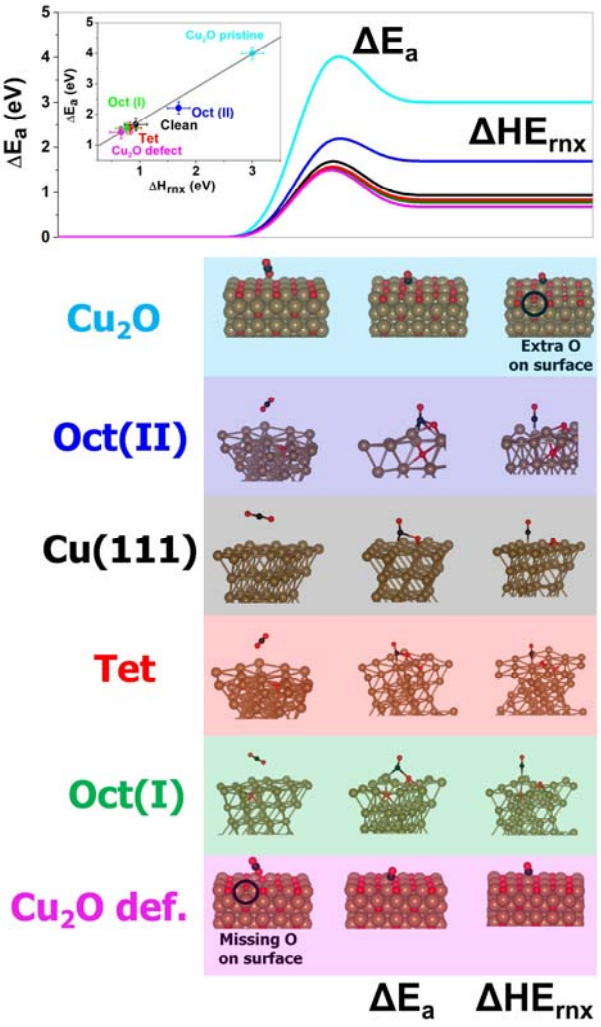

Figure 5: A Calculation of the adsorption barrier and heat of reaction of different copper structures. The inset shows the E_a versus H_{rxn}.

Similar, yet more dramatic behavior, can also be seen for the cuprous oxide surface. For this purpose we chose to explore a Cu_2O(110) surface. On the pristine surface the calculated E_a is 4 eV with H_{rxn} = 3 eV due to the formation of extra oxygen on the surface, yielding a high-energy local CuO-like motif[36]. However, introducing an oxygen vacancy on the Cu_2O(110)

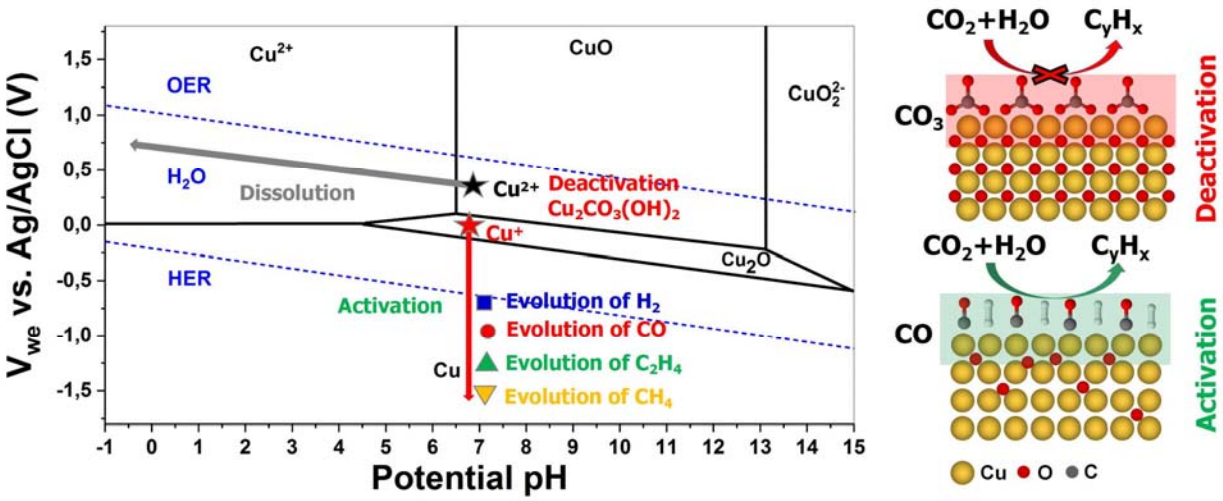

Figure 6: Performance resume with the Puorbaix diagram and the different copper oxide catalysts behavior found during the experiments and schematic of the catalyst activation-deactivation due to the formation of carbonates in Cu^{2+} like electrode.

surface lowers E_a to 1.20 eV with H_{rxn} = 0.61 eV, as in this case the oxygen adatom formed during CO_2 decomposition can fill the lattice oxygen vacancy. These results are summarized in Figure 5, where the shows E_a is plotted vs. H_{rxn} indicating that the most suitable structure for the effective dissociation of CO_2 are metallic surface with dissolved subsurface oxygen or partially reduced metal oxides, with oxygen vacancies. Thus, these results indicate the copper electrode must be (partially) reduced to facilitate the dissociative adsorption of CO_2, in agreement with our findings based on the *in situ* spectra at the Cu $L_{2,3}$-edges and the Cu K-edge. These computations suggest that the dissociative proton-consuming reactive adsorption of CO_2 to produce CO on copper catalysts take places more readily on a non-stoichiometric copper surface, predicting the lowest barrier for CO_2 decomposition is on the non-stoichiometric oxygen-clean $Cu_{2+\delta}O$ surfaces. However, the Pourbaix diagram of copper predicts (see Figure 6) that the copper oxide is not stable under most of the cathodic potentials at different pHs, as the *in situ* XAS-EXAFS measurements proved, which is in the nature of the high overpotential observed in Cu catalysts under CO_2RR conditions.

Thus, taking into account the discussed experiments and the calculations of the dissociation barrier of CO_2 onto different copper surfaces, it is obvious that the hydrogenation of CO takes places when copper is locally reduced (and/or when oxygen vacancies are involved in the reaction) allowing the dissociative adsorption of CO_2 onto the surface. *In situ* X-ray spectroscopies, both XAS and EXAFS, indicate that copper carbonates are generated on Cu^{2+} oxides hindering effective charge transport due to the formation of a passivation layer. This layer can be eliminated at low pH conditions due to the introduction of an acidic electrolyte in the cell or by applying potential; if the contact resistance is not too high (i.e. the high contact resistance can be lowered increasing the electrode area). Thus, Cu^{2+} is likely not active in the cathodic reduction of CO_2 into valuable hydrocarbons due to its deactivation as a consequence of the

formation of a passivating copper carbonate layer as shown schematically in the Figure 6. Meanwhile, if the electrode is in the form of Cu^{+}, it undergoes the dissociative adsorption of CO_2 onto oxygen vacancies present on the surface till the HER is reached. Under HER the Cu^{+} oxide is reduced to form Cu^{0}, due to the low stability of copper oxide under these conditions, as the Pourbaix diagram shows (Figure 6). After that, the first hydrocarbon product evolving is C_2H_4 due to a dimerization process and finally CH_4 at higher cathodic potential due to protonation effects on a proton rich interface indicating high selectivity to C_2 for this type of electrode. A schematic with the activation and deactivation scheme of the catalyst surface induced by the formation of different intermediates is depicted in Figure 6 as well, which summarizes the overall process.

Conclusions

Redox-active copper catalysts were accurately prepared yielding high selectivity to the C_2 hydrocarbons formation during the CO_2RR. The combination of *in situ* XAS/EXAFS, and GC product analysis provided direct evidence on the mechanisms governing the reduction of CO_2 to industrial valuable C_2 and C_1 products on electrochemically prepared Cu electrodes with different initial redox states. It was found that the catalyst surface, subsurface and bulk are affected by the presence of copper carbonates that inhibit the adsorptive dissociation of CO_2. Instead, the key dissociative proton-consuming reactive adsorption of CO_2 requires the formation of a reduced or partially-reduced electrode. Once dissociative CO_2 adsorption occurs the hydrogenation of CO is controlled as a consequence of a dimerization and protonation processes yielding C_2 and C_1 valuable products, respectively.

Supporting Information

Additional supporting figures (Figure S1-S4) for the in situ reactions in 5 mM $KClO_4$ (saturated in N_2 gas) and 5 mM $KHCO_3$ (saturated in CO_2), dissociative proton-consuming reactive adsorption of CO_2, dissolution of copper carbonates in presence of 100 mM $HClO_4$ (saturated in N_2 gas), density of current depending on the applied potential in 100 mM $KHCO_3$ saturated in CO_2 for the different CuO_x catalysts.

In situ electrochemical cell fabrications details.

Calculations of the Faradaic efficiency of gas products.

Acknowledgment

This work was supported by the Ministry of Education and Science of the Russian Federation (RFMEFI61614X0007) and the Bundesministerium für Bildung und Forschung (BMBF-05K14EWA) through the joint Russian-German research project “SYnchrotron and NEutron STudies for Energy Storage (SYNESTESia).” We thank DAAD for financial support in the framework of Taiwanese-German collaboration (projects ID 57218279 and 57392335).

C.H.C. acknowledges financial support from projects 104-2112-M-032-005-MY2 and 105-2911-I-032-501. D.G. and B.R.C. and P.S. acknowledge funding from BMBF under grants 03SF0523C and 03SF0523A -'CO2EKAT' and eEthylene: 033RCOO4D and 033RCOO4C. D.G. B.R.C. also appreciate the financial support of the European Research Council under grant ERC-OPERANDOCAT (ERC-725915).We acknowledge Höchstleistungsrechenzentrum Stuttgart (HLRS) for access to the supercomputer HazelHen.

References:

1. Schlögl, R. The role of chemistry in the energy challenge. *ChemSusChem* **2018,** 3(2), 209-222, DOI 10.1002/cssc.200900183.
2. Qiao, J. et al. A review of catalysts for the electroreduction of carbon dioxide to produce low-carbon fuels. *Chem. Soc. Rev.* **2014**, 43(2), 631-675, DOI 10.1039/C3CS60323G.
3. Schlögl, R. The solar refinery. In Chemical Energy Storage. *De Gruyter*, **2013**, 1-34.
4. Kondratenko, E. et al. Status and perspectives of CO_2 conversion into fuels and chemicals by catalytic, photocatalytic and electrocatalytic processes. *Ener. & Envir. Sci.* **2013**, 6(11), 3112-3135, DOI 10.1039/C3EE41272E.
5. Kuhl, K. P. et al. Electrocatalytic conversion of carbon dioxide to methane and methanol on transition metal surfaces. *JACS* **2014**, 136(40), 14107-14113, DOI 10.1021/ja50579.
6. Khezri, B.; Fisher, A. C.; Pumera, M. CO_2 reduction: the quest for electrocatalytic materials. *J. of Mat. Chem. A* **2017**, 5(18), 8230-8246, DOI 10.1039/C6TA09875D.
7. Hori, Y.; Kikuchi, K.; Suzuki, S. Production of CO and CH_4 in electrochemical reduction of CO_2 at metal electrodes in aqueous hydrogencarbonate solution. *Chem. Lett.* **1985**, 14(11), 1695-1698, DOI 10.1246/cl.1985.1695.
8. Hori, Y. et al. Production of methane and ethylene in electrochemical reduction of carbon dioxide at copper electrode in aqueous hydrogencarbonate solution. *Chem. Lett.* **1986**, 15(6), 897-898, DOI 10.1246/cl.1986.897.
9. Kas, R. et al. Electrochemical CO_2 reduction on Cu_2O-derived copper nanoparticles: controlling the catalytic selectivity of hydrocarbons.*Phys. Chem. Chem. Phys.* **2014**, 16(24), 12194-12201, DOI 10.1039/C4CP01520G.
10. Hori, Y.; Murata, A.; Takahashi, R. Formation of hydrocarbons in the electrochemical reduction of carbon dioxide at a copper electrode in aqueous solution. *Far. Trans.* **1989**, 85(8), 2309-2326, DOI 10.1039/F19898502309.
11. Jermann, B.; Augustynski, Long-term activation of the copper cathode in the course of CO_2 reduction. J. *Electro. Act.* **1994**, 39(11-12), 1891-1896, DOI 10.1016/0013-4686(94)85181-6.
12. Hori, Y. et al. Selective formation of C2 compounds from electrochemical reduction of CO_2 at a series of copper single crystal electrodes. *The J. of Phys. Chem. B* **2002**, 106(1), 15-17, DOI 10.1021/jp013478d.
13. Li, C. W.; Kanan, M. W. CO_2 reduction at low overpotential on Cu electrodes resulting from the reduction of thick Cu_2O films. *JACS* **2012**, 134(17), 7231-7234, DOI 10.1021/ja3010978.

14. Ma, M.; Djanashvili, K.; Smith, W. A. Controllable hydrocarbon formation from the electrochemical reduction of CO_2 over Cu nanowire arrays. *Ang. Chem. Int. Ed.* **2016**, 128(23), 6792-6796, DOI 10.1002/ange.201601282.
15. Kim, D. et al. Insights into an autonomously formed oxygen-evacuated Cu_2O electrode for the selective production of C_2H_4 from CO_2. *Phys. Chem. Chem. Phys.* **2015**, 17(2), 824-830, DOI 10.1039/C4CP03172E.
16. Mistry, H. et al. Highly selective plasma-activated copper catalysts for carbon dioxide reduction to ethylene. *Nat. Comm.* **2016**, 7, 12123, DOI 10.1038/ncomms12123.
17. Reske, R. et al. Particle size effects in the catalytic electroreduction of CO_2 on Cu nanoparticles. *JACS* **2014**, 136(19), 6978-6986, DOI 10.1021/ja500328k.
18. Kas, R. et al. Three-dimensional porous hollow fibre copper electrodes for efficient and high-rate electrochemical carbon dioxide reduction. *Nat. Comm.* **2016**, 7, 10748, DOI 10.1038/ncomms10748.
19. Loiudice, A.; Lobaccaro, P.; Kamali, E. A.; Thao, T.; Huang, B. H.; Ager, J. W.; Buonsanti, R. Tailoring copper nanocrystals towards C2 products in electrochemical CO_2 reduction. *Ang. Chem. Int. Ed.* **2016**, 55(19), 5789-5792, DOI 10.1002/anie.201601582.
20. Gao, D. et al. Plasma-Activated Copper Nanocube Catalysts for Efficient Carbon Dioxide Electroreduction to Hydrocarbons and Alcohols. *ACS Nano* **2017**, 11(5), 4825-4231, DOI 10.1021/acsnano.7b01257.
21. Grosse, P. et al. Dynamic Changes in the Structure, Chemical State and Catalytic Selectivity of Cu Nanocubes during CO_2 Electroreduction: Size and Support Effects. *Ang. Chem. Int. Ed.* **2018**, 130(21), 6300-6305, DOI 10.2002/ange.201802083.
22. Yang, K. D. et al. Morphology-Directed Selective Production of Ethylene or Ethane from CO_2 on a Cu Mesopore Electrode. *Ang. Chem. Int. Ed.* **2017**, 56(3), 796-800, DOI 10.1002/anie.201610432.
23. Huan, T. N. et al. Porous dendritic copper: an electrocatalyst for highly selective CO_2 reduction to formate in water/ionic liquid electrolyte. *Chem. Sci.* **2017**, 8(1), 742-747, DOI 10.1039/C6SC03194C.
24. Itkis, D. M. et al. Probing operating electrochemical interfaces by photons and neutrons. *ChemElectroChem* **2015**, 2(10), 1427-1445, DOI 10.1002/celc.201500155.
25. Velasco-Vélez, J. J. et al. The structure of interfacial water on gold electrodes studied by x-ray absorption spectroscopy. *Science* **2014**, 1259437, DOI 10.1126/science.1259437.
26. Velasco-Vélez, J. J. et al.Trends in reactivity of electrodeposited 3d transition metals on gold revealed by operando soft x-ray absorption spectroscopy during water splitting. *J. of Phys. D: App. Phys.* **2016**, 50(2), 024002, DOI 10.1088/1361-6463/50/2/024002.
27. Velasco-Vélez, J. J. et al. The Electro-Deposition/Dissolution of $CuSO_4$ Aqueous Electrolyte Investigated by In Situ Soft X-ray Absorption Spectroscopy. *The J. of Phys. Chem. B* **2018**, 122(2), 780-787, DOI 10.1021/acs.jpcb.7b06728.
28. Kuhl, K. P. et al. New insights into the electrochemical reduction of carbon dioxide on metallic copper surfaces. *Ener. & Environ. Sci.* **2012**, 5(5), 7050-7059, DOI 10.1039/C2EE21234J.

29. Velasco-Velez, J. J. et al. Drift modeling of electrically controlled nanoscale metal–oxide gas sensors. *IEEE EDL* **2008**, *29*(7), 677-680, DOI 10.1109/LED.2008.2000605.
30. Cook, R. L.; MacDuff, R. C.; Sammells, A. F. On the electrochemical reduction of carbon dioxide at in situ electrodeposited copper. *JES* **1988**, 135(6), 1320-1326, DOI 10.1149/1.2095972.
31. Lee, J.; Tak, Y. Electrocatalytic activity of Cu electrode in electroreduction of CO_2. *Electro. Act.* **2001**, 46(19), 3015-3022, DOI 10.1016/S0013-4686(01)00527-8.
32. Lee, X.; Sun, L.; Den, W. Q. Theoretical Investigation of CO_2 Adsorption and Dissociation on Low Index Surfaces of Transition Metals. *The J. of Phys. Chem. C* **2018**, 122(15), 8306-8314, DOI 10.1021/acs.jpcc.7b12660.
33. Soon, A.; Todorova, M.; Delley, B.; Stampfl, C. Oxygen adsorption and stability of surface oxides on Cu (111): A first-principles investigation. *Phys. Rev. B* **2016**, 73(16), 165424, DOI 10.1103/PhysRevB.73.165424.
34. Knop-Gericke et al. Characterization of active phases of a copper catalyst for methanol oxidation under reaction conditions: an in situ X-ray absorption spectroscopy study in the soft energy range. *Top. in Cat.* **2001**, 15(1), 27-34 (2001), DOI 10.1023/A:1009015728467.
35. Eilert, A. et al. Subsurface Oxygen in Oxide-Derived Copper Electrocatalysts for Carbon Dioxide Reduction. *The J. of Phys. Chem. Lett.* **2016**, 8(1), 285-290, DOI 10.1021/acs.jpclett.6b02273.
36. Greiner, M. T. et al. Ethylene epoxidation at the phase transition of copper oxides. *JACS* **2017**, 139(34), 11825-11832, DOI 10.1021/jacs.7b05004.
37. Giannozzi, P. et al. QUANTUM ESPRESSO: a modular and open-source software project for quantum simulations of materials. *J. of Phys.: Cond. Matt.* **2009**, 21(39), 395502, DOI 10.1088/0953-8984/21/39/395502.
38. Perdew, J. P.; Burke, K.; Ernzerhof, M. Generalized gradient approximation made simple. *Phys. Rev. Lett.* **1996**, 77(18), 3865, DOI 10.1103/PhysRevLett.77.3865.
39. Dal Corso, A. Pseudopotentials periodic table: From H to Pu. *Comp. Mat. Sci.* **2014**, 95, 337-350, DOI 10.1016/j.commatsci.2014.07.043.
40. Otero-de-la-Roza, A.; Johnson, E. R. Van der Waals interactions in solids using the exchange-hole dipole moment model. *The J. of Chem. Phys.* **2012**, 136(17), 174109, DOI 10.1063/1.4705760.
41. Marzari, N. et al. Thermal contraction and disordering of the Al (110) surface. *Phys. Rev. Lett.* **1999**, 82(16), 3296, DOI 10.1103/PhysRevLett.82.3296.
42. Hall, A. S.; Yoon, Y.; Wuttig, A.; Surendranath, Y. Mesostructure-induced selectivity in CO_2 reduction catalysis. *JACS* **2015**, 137(47), 14834-14837, DOI 10.1021/jacs.5b08259.
43. Kurian, R.; Kunnus K.; Wernet P.; Butorin S. M.; Glatzel P.; de Groot F. Intrisic deviation in fluorescence yield detected x-ray absorption spectroscopy: the case of the transition metal $L_{2,3}$ edges. *J. of Phys.: Cond. Matt.* **2012**, 24(45), 452201, DOI 10.1088/0953-8984/24/45/452201.

For Table of Contents Use Only

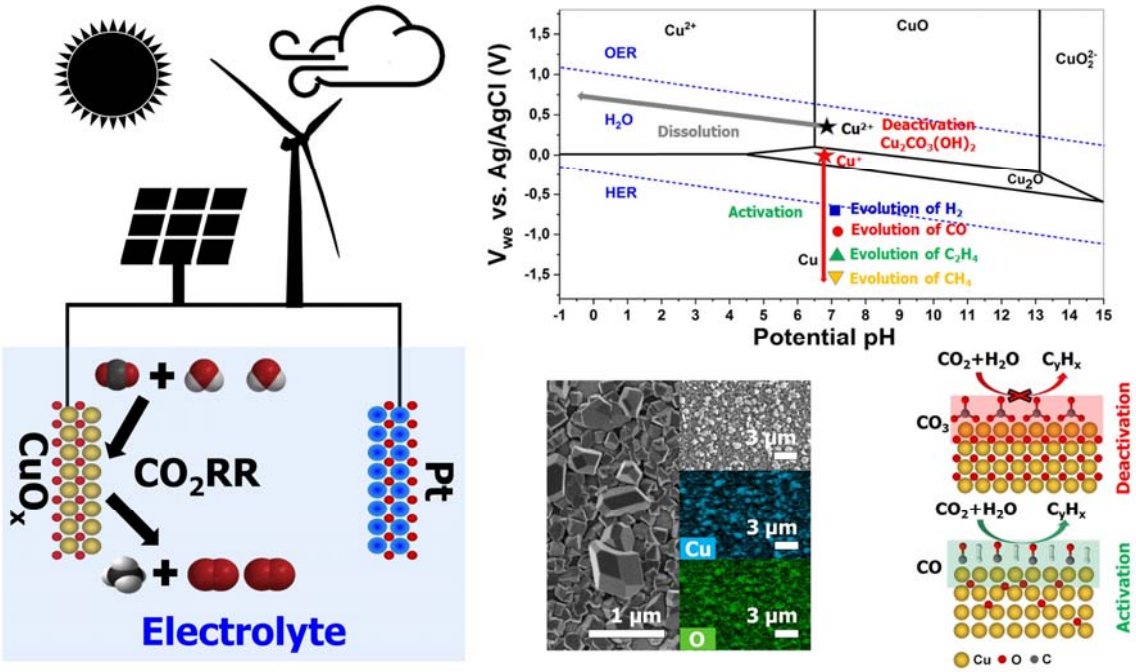

Synopsis: The electronic factor making copper unique in the electrochemical reduction of CO_2 into valuable hydrocarbons was revealed using different redox-active copper catalysts with accurately prepared oxidation state by means of *in situ* X-ray spectroscopy.

Supplementary information

The role of the copper oxidation state in the electrocatalytic reduction of CO_2 into valuable hydrocarbons

Juan-Jesús Velasco-Vélez[1,2]*, Travis Jones[2], Dunfeng Gao[3,4], Emilia Carbonio[2], Rosa Arrigo[5,6], Cheng-Jhih Hsu[7], Yu-Cheng Huang[7,8], Chung-Li Dong[7], Jin-Ming Chen[8], Jyh-Fu Lee[8], Peter Strasser[9], Beatriz Roldan Cuenya[3,4], Robert Schlögl[1,2], Axel Knop-Gericke[1,2], Cheng-Hao Chuang[7]*

[1]Department of Heterogeneous Reactions, Max Planck Institute for Chemical Energy Conversion, Stiftstraße 34-36, Mülheim an der Ruhr 45470, Germany
[2]Department of Inorganic Chemistry, Fritz-Haber-Institut der Max-Planck-Gesellschaft, Faradayweg 4-6, Berlin 14195, Germany
[3] Department of Physics, Ruhr-University Bochum, Universitätstraße 150, 44780 Bochum, Germany
[4]Department of Interface Science, Fritz-Haber-Institute of the Max-Planck Society, Faradayweg 4-6, 14195 Berlin, Germany
[5]Diamond Light source Ltd., Harwell Science & Innovation Campus, Didcot, Oxfordshire OX 11 0DE, UK
[6]School of Environment and Life Sciencesm, University of Salford, Cockcroft building, M5 4WT, Manchester, UK
[7]Department of Physics, Tamkang University, No. 151 ,Yingzhuan Rd., Danshui Dist, New Taipei City 25137, Taiwan.
[8]National Synchrotron Radiation Research Center, No. 101, Hsin Ann Rr., East District., Hsinchu 30076, Taiwan
[9]Department of Chemistry, Chemical Engineering Division, Technical University Berlin, Straße des 17. Juni 124, 10623 Berlin, Germany

*Corresponding authors: velasco@fhi-berlin.mpg.de, chchuang@mail.tku.edu.tw

Number of pages: 5

Number of Figures: 4

In situ flow cell for X-ray spectroscopy

The *in situ* EC flow liquid cell was operated on the main chamber of the beamline 20A1 end station of the National Synchrotron Radiation Research Center (NSRRC) in Hsinchu (Taiwan) with a background pressure of ~10^{-8} mbar while the aqueous electrolyte circulated on the back side of a SiN_x membrane 100 nm thick (from the company Norcada, Edmonton, Canada). Theeffective area of the working electrode was ~2 mm^2. This membrane is used as working electrode and membrane to separate the liquid form the vacuum side. Hard X-ray absorption measurements at the Cu K-edge were performed at the beamline BL17C1 of the National Synchrotron Radiation Research Center (NSRRC) in Hsinchu (Taiwan). The photon source consists of a 25 poles wiggler (W20) with 20 cm period length and a focus spot size of 2 mm x 6 mm. The excitation energy ranges from 4.8 keV up to 14.2 keV. The signal was collected in fluorescence yield mode using an ionization chamber detector. A similar cell to the used in beamline 20A1 was located in the BL17C hutch at 1 bar in air with an effective area of the working electrode of ~36 mm^2. The flow of liquid was assured with a peristaltic micro pump, flowing continually around 1 ml/min of electrolyte. In the Si_3N_4 membrane a thin Au/Ti thin film was deposited by sputtering using a Cressington 208HR sputter-deposition system. First of all, 3 nm-thick adhesion layer of Ti (99.99%, Elektronen-Optik-Service GmbH, Dortmund, Germany) was deposited in a 0.1 mbar Ar atmosphere at a current of 40 mA during 30 s. After that, a 20 nm-film of Au (99.99%, Elektronen-Optik-Service GmbH, Dortmund, Germany) was deposited in a 0.1 mbar Ar atmosphere at a current of 40 mA during 140 s. It yields the formation of a homogenous polycrystalline thin film used as working electrode20 nm thick on a SiN_x membrane (100 nm), which yields a total signal transmission of ~74% of the incoming X-ray photons. The X-ray transmission through this membrane is estimated to be approximately equal to 80% of the incoming X-ray. The main body of the cell is made of polyether ether ketone (PEEK) which is electrically insulator and chemically inert.

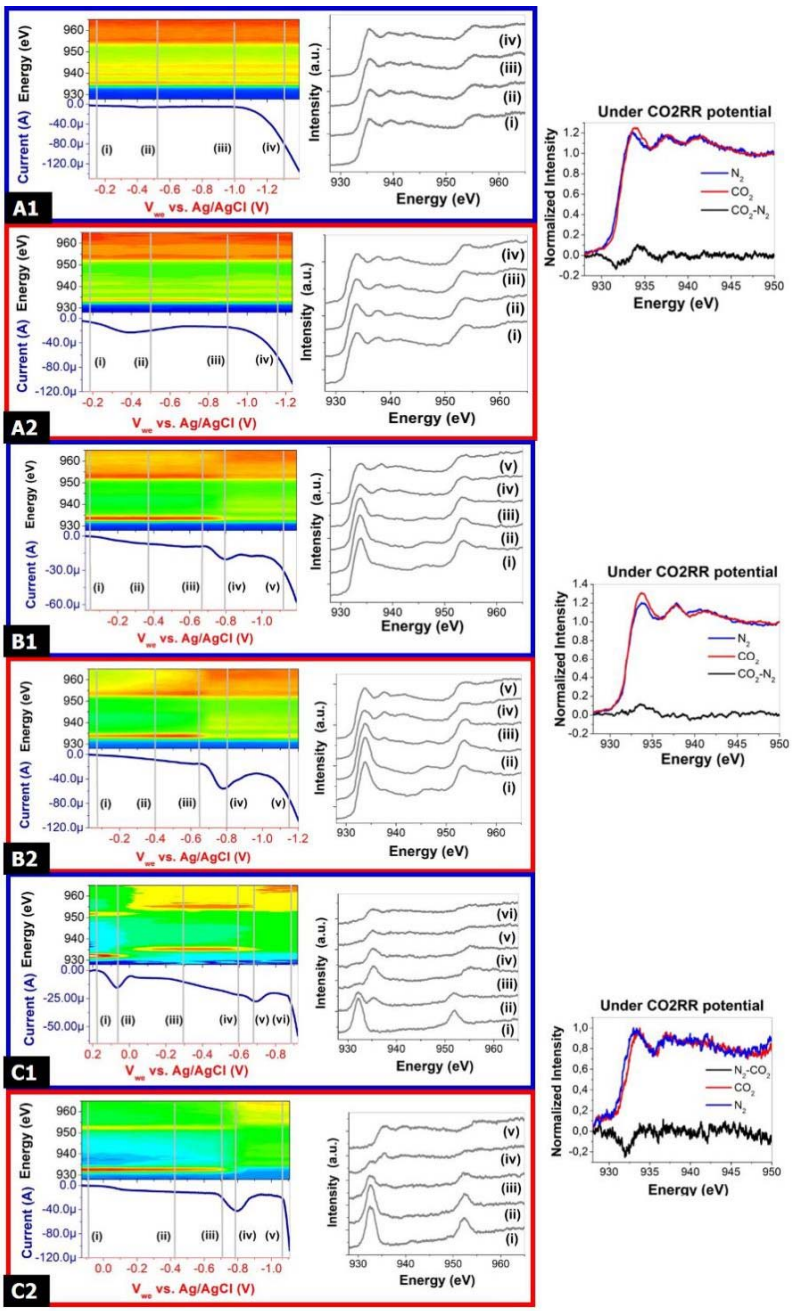

Figure S1: Cu $L_{2,3}$-edges spectra depending on the cathodic polarization in the presence of different electrolytes and initial oxidation state: **A** Cu^0 catalyst **A1** 5 mM $KClO_4$ saturated with N_2(gas) and **A2** 5 mM $KHCO_3$ saturated with CO_2(gas). **B** Cu^+ catalyst **B1** 5 mM $KClO_4$ saturated with N_2(gas) and **B2** 5 mM $KHCO_3$ saturated with CO_2(gas). **C** Cu^{2+} catalyst **C1** 5 mM $KClO_4$ saturated with N_2(gas) and **C2** 5 mM $KHCO_3$ saturated with CO_2(gas). Side graphics are the Cu L-edge spectra under the highest cathodic polarization with the different electrolytes in order to compare the formation of surface/sub-surface oxygen species.

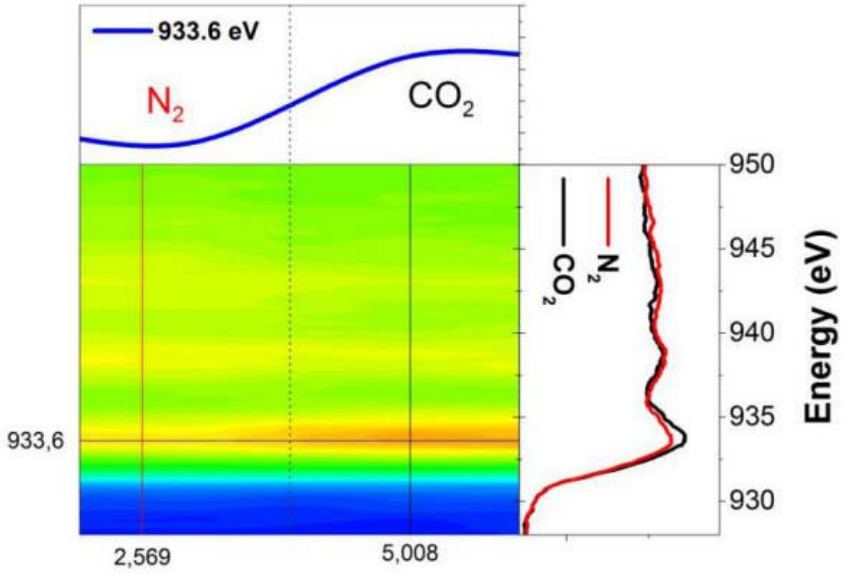

Figure S2: Cu L_3-edge of Cu^0 catalyst in presence of N_2 and CO_2 shows the existence of a slightly increase of Cu^+ species in presence of CO_2 ascribed to the existence of dissociative proton-consuming reactive adsorption of CO_2 on copper yielding chemisorbed CO.

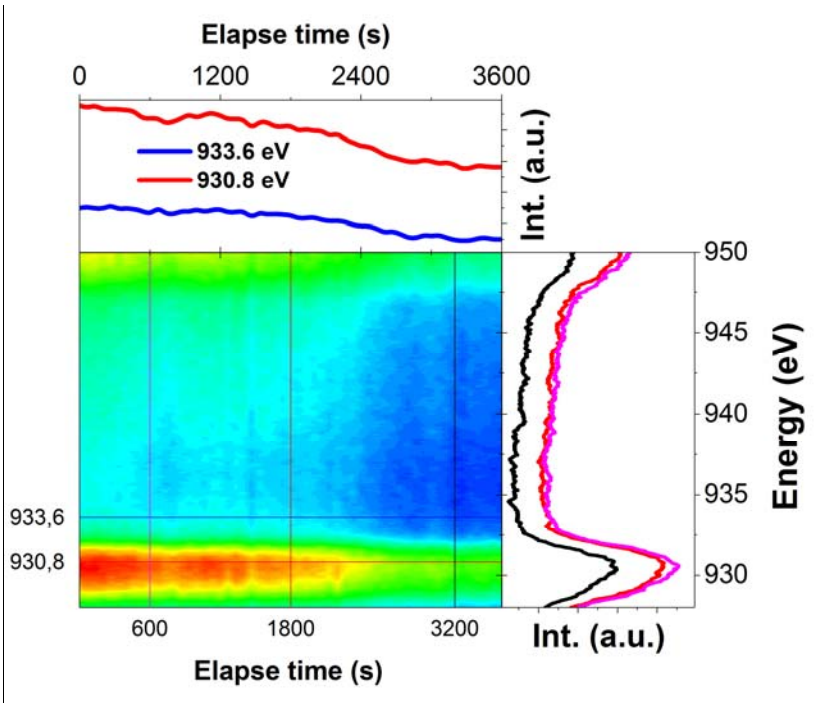

Figure S3: Cu L_3-edge depending on elapse time of copper carbonates species in presence of 100 mM $HClO_4$ acidic media.

Calculation of the Faradaic efficiency of gas products:

$$f_{gas} = \frac{f_{flow} \times c_{gas} / V_m \times n \times F}{I \times 60} \times 100$$

f_{gas}: Faradaic efficiency of gas product, %;

f_{flow}: flow rate of CO_2, mL min^{-1};

I: electrolysis current at 60 min, A;

c_{gas}: volume ratio of gas product, determined by online GC;

V_m: the molar volume of an ideal gas at 1 atmosphere of pressure, 22400 mL mol^{-1};

n: number of transferred electrons for certain product;

F: Faradaic constant, 96485 C mol^{-1}.

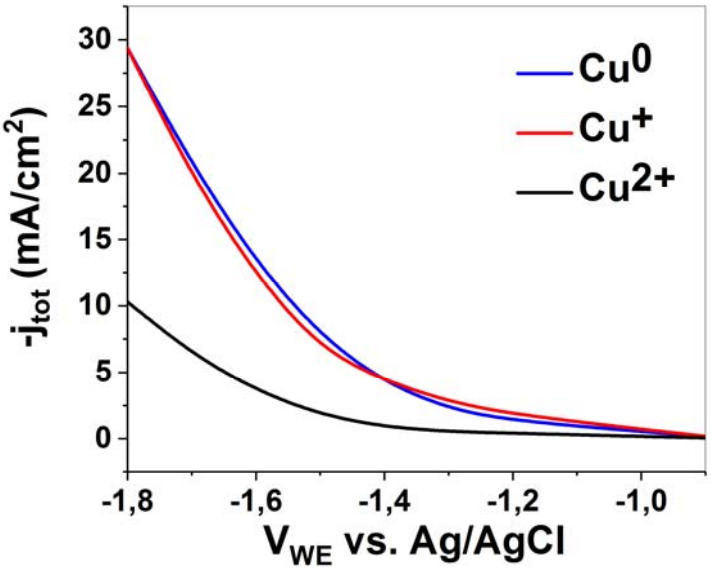

Figure S4: Density of current for Cu^0, Cu^+ and Cu^{2+} depending on the applied potential in 100 mM $KHCO_3$ saturated in CO_2.